Real-time optical reflectometry enabled by amplified dispersive Fourier transformation

Keisuke Goda,[a] Daniel R. Solli, and Bahram Jalali
Department of Electrical Engineering, University of California, Los Angeles, California 90095, USA

(Received 6 June 2008; accepted 3 July 2008; published online 23 July 2008)

The axial scan rate of optical frequency-domain reflectometry and optical coherence tomography can be increased to megahertz frequencies by dispersive Fourier transformation. However, the fundamental connection between dispersion and loss creates a trade-off between detection sensitivity and acquisition speed. Here we circumvent this predicament by using distributed Raman postamplification of the reflection from the sample. The Raman amplification enables measurement of weak signals, which are otherwise buried in detector noise. It extends the depth range without sacrificing the acquisition speed. Single-shot imaging with improved sensitivity at an axial scan rate of 36.6 MHz is demonstrated. © *2008 American Institute of Physics*. [DOI: 10.1063/1.2963974]

Optical coherence tomography[1,2] (OCT) has proven to be a powerful technique for studying tissue morphology.[3,4] Frequency-domain OCT has been demonstrated to provide higher acquisition speed than time-domain OCT.[5] As of today, frequency-domain OCT methods such as Fourier-domain OCT (Ref. 6) and swept-source OCT (Ref. 4) can achieve an axial scan rate of more than 10 kHz with ease.

Among the two frequency-domain approaches, the image acquisition speed of Fourier-domain OCT is limited by the data acquisition speed of the array detector (e.g., a charge coupled device or complementary metal oxide semiconductor),[6] which is typically between 10 and 100 kHz. In other words, there is a tradeoff between the spectral resolution and axial scan rate. On the other hand, swept-source OCT does not require an optical spectrometer because the wavelength is known for each time sample, leading to a higher axial scan rate than Fourier-domain OCT (up to 100 kHz as of today[4]); however, the bandwidth, and hence the axial resolution, is limited by the tuning range of the laser, and the broadening of the instantaneous linewidth due to the rapid sweep rate limits the depth range.

Dispersive Fourier transformation (FT) exploits the mathematical equivalence between paraxial diffraction and temporal dispersion.[7] Its ability to map spectral information into a temporal waveform has been used in spectroscopy,[8,9] optical frequency-domain reflectometry (OFDR),[10] and OCT.[11] Measuring the spectrum in Fourier-domain OCT using dispersive FT avoids the issues mentioned above by eliminating the diffraction grating and detector array.[10,11] These elements are replaced by a dispersive fiber, a single detector and, a digitizer. This simplifies the system and, more importantly, enables fast real-time image acquisition. This method also allows a larger bandwidth to be used compared with swept-source OCT. However, the loss in the dispersive medium, which at the most basic level is caused by the intimate connection between dispersion and loss described by the Kramers–Kronig relations,[7] limits the detection sensitivity as well as the depth range.

The latter can be understood by recognizing that by virtue of spectrum-to-time conversion, the spectral resolution (which determines the depth range) is fixed by the temporal resolution of the electrical detection system. Stated differently, the electrical bandwidth of the digitizer limits the spectral resolution, a relation given by $\Delta f = 0.35\lambda_0^2/cDf_{\mathrm{dig}}$,[8] where Δf is the spectral resolution, λ_0 is the center wavelength, c is the speed of light in vacuum, D is the total group-velocity dispersion, and f_{dig} is the input bandwidth of the real-time digitizer. The product of $\Delta f \times D$ is fixed by the bandwidth of the digitizer; hence, to increase the optical resolution (i.e., to increase the depth range), one is forced to increase the total group-velocity dispersion, D. However, this comes at the expense of increased optical loss and reduced detection sensitivity. Increasing the detection bandwidth for higher spectral resolution and lower loss is not desirable because the electrical gain-bandwidth product and detector thermal noise reduce detection sensitivity. The loss in the dispersive element is, therefore, the central problem in high sensitivity detection. This implies that a longer integration time must be used, limiting the axial scan rate. Thus, the loss in the dispersive element creates a tradeoff between the sensitivity and scan rate. Increasing the laser power is not an attractive solution because it can cause damage to the tissue[12] or unwanted nonlinear signal distortion.

Our approach is different from previously demonstrated dispersive Fourier-domain OCT (Ref. 11) and OFDR (Ref. 10) through the use of internal amplification in the dispersive element. By compensating for the loss in the dispersive element, it overcomes the tradeoff between the detection sensitivity (and hence the imaging depth) and acquisition speed. For optimum performance, we perform this function in the sample arm of the Michelson interferometer (Fig. 1) in order to increase the strength of the signal reflected from the sample. This enhances the interference contrast in the interference fringe that is otherwise buried in detector noise and, hence, improves the imaging sensitivity. Distributed amplification during the process of the dispersive FT has previously been used to demonstrate real-time spectroscopy.[8,9]

The desirable features for a dispersive element are high total dispersion, low loss, large optical bandwidth, smooth dispersion over the bandwidth, and commercial availability. Dispersion compensation fiber (DCF) offers an optimum combination of these parameters and is our preferred choice. While the loss can also be compensated by discrete optical amplifiers such as erbium-doped fiber amplifiers or even

[a]Electronic mail: goda@ee.ucla.edu.

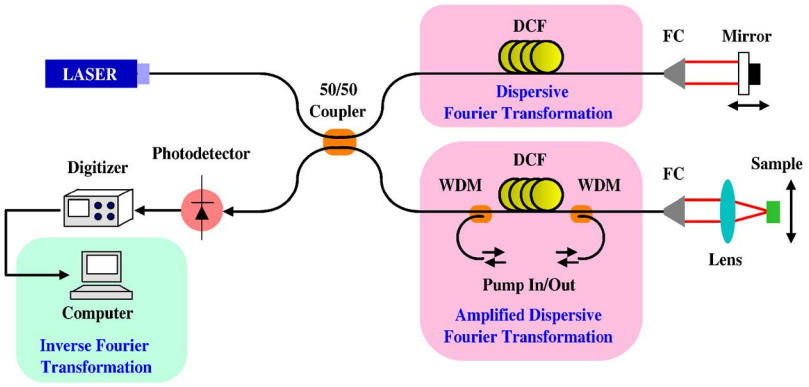

FIG. 1. (Color online) Schematic of the experimental Raman-amplified dispersive Fourier-transform reflectometer. WDM: wavelength-division multiplexer; DCF: dispersion compensation fiber; FC: fiber collimator. Each interferometer arm has a DCF module with equal round-trip dispersion of −1316 ps/nm and loss of 7.6 dB. Dispersive FT is performed in the DCF of each arm, mapping the spectrum into a temporal waveform. During the dispersive Fourier transformation in the sample arm, distributed Raman amplification is implemented by pumping it with two diode lasers. The Raman pumps are injected into and removed from the DCF by the WDMs. Inverse FT is performed on the digitizer output to map the temporal waveform into the depth profile.

semiconductor optical amplifiers, distributed Raman amplification within the dispersive DCF is superior because it maintains a relatively constant signal level throughout the FT process. This important property maximizes the signal-to-noise-and-distortion ratio by keeping the signal power away from low power (noisy) and high power (nonlinear) regimes. Incidentally, this advantage of distributed Raman amplification over discrete amplification is known in long haul fiber optic communication links.[13]

Our Raman-amplified dispersive FT reflectometer is different from previously demonstrated techniques for improving the sensitivity of OCT by optical postamplification of sample reflections[14,15] through (1) the use of dispersive FT and (2) the use of distributed Raman amplification as opposed to discrete semiconductor optical amplifiers. In addition to a lower noise figure, Raman amplification also has a more flexible gain spectrum than semiconductor amplifiers or erbium-doped fiber amplifiers: in an amorphous medium such as glass, it is naturally broadband. The gain spectrum can be further broadened by using multiwavelength pump lasers, and, surprisingly but fortuitously, extremely broadband gain spectra can be realized using incoherent pump sources.[9] This is highly desirable because a large optical bandwidth results in high axial image resolution in OCT and OFDR. Raman-amplified dispersive elements also eliminate the need for a high power source.

The schematic of the Raman-amplified reflectometer is shown in Fig. 1. The optical source is a mode-locked femtosecond laser (Precision Photonics) with a 36.6 MHz repetition rate. It is filtered and amplified by an erbium-doped fiber amplifier (PriTel), producing the spectrum shown in Fig. 2. Pulses with a 2.7 kW peak power and a 150 fs pulse duration are injected into the Michelson interferometer where the reference and a sample arms contain a mirror and a sample at their ends, respectively. Each arm has a DCF module with an equal round-trip dispersion of −1316 ps/nm and loss of 7.6 dB. The DCF performs dispersive FT to map the spectrum to a temporal waveform. The equal dispersion balances the dispersive FTs in the arms. The reflections from the sample and mirror interfere at the 50/50 fiber coupler, resulting in a spectral fringe in which the depth profile of the sample is encoded. A variable attenuator and a polarization controller are used in the reference arm to optimize the spectral interference formed by the reflections from the sample and reference arms. The mirror in the reference arm is placed on a translation stage with a micrometer actuator to adjust the time delay between the return pulses in the sample and reference arms. Distributed Raman amplification is implemented in the DCF by pumping it with two 98.5 mW diode lasers with center wavelengths of 1470 and 1480 nm. The Raman pumps used to pump the DCF module are diode lasers (Furukawa) designed for distributed Raman amplification in telecommunications systems. Based on the group-velocity dispersion of −1316 ps/nm and the digitizer sampling rate of 50 GS/s, the spectral resolution of the Raman-amplified reflectometer is found to be $\delta\lambda = 30.4$ pm (assuming that at least two sampling points are required to resolve spectra), which corresponds to a depth range of 20.6 mm in air. The interferometer output is detected by an ac-coupled AD-50ir amplified photodetector (Newport) with 50 ps response time and is captured with a 50 GS/s real-time DPO71604 digitizer (Tektronix) with a 16 GHz bandwidth. Inverse FT is performed on the digitizer output to map the time-domain waveform into the depth profile. The axial scan rate is equivalent to the repetition rate of the laser (36.6 MHz), which is the highest axial scan speed ever reported in OFDR and OCT. It is two orders of magnitude faster than conventional OFDR (Ref. 16) and OCT.[4]

The basic performance of the Raman-amplified reflectometer is shown in Fig. 2. *Single-shot* OCT point spread functions with a mirror in the sample arm at various imaging depths are evident in the figure. In this proof-of-principle demonstration, the axial resolution (227 μm) is limited by the modest bandwidth of the source (15 nm) centered at 1583.8 nm, but we emphasize that this is not an inherent limitation of the technique and can be significantly improved

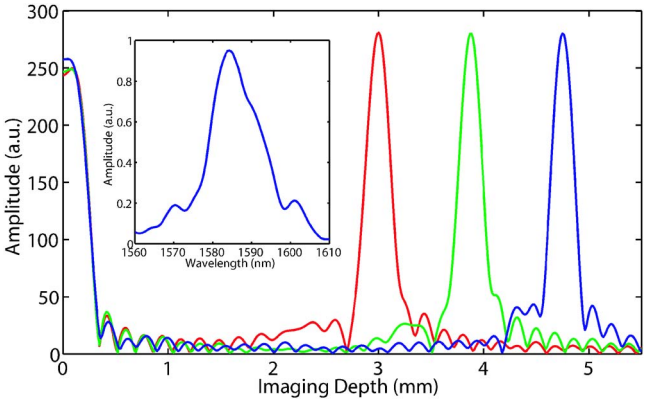

FIG. 2. (Color online) Basic performance of the Raman-amplified reflectometer showing the spectrum of the optical source and single-shot point spread functions at various imaging depths. After filtering and amplification, a spectrum centered at 1583.8 nm with a full width at half maximum bandwidth of 15.0 nm is obtained. The axial resolution (227 μm) is limited by the modest bandwidth of the source (15.0 nm) centered at 1583.8 nm in this proof-of-principle demonstration.

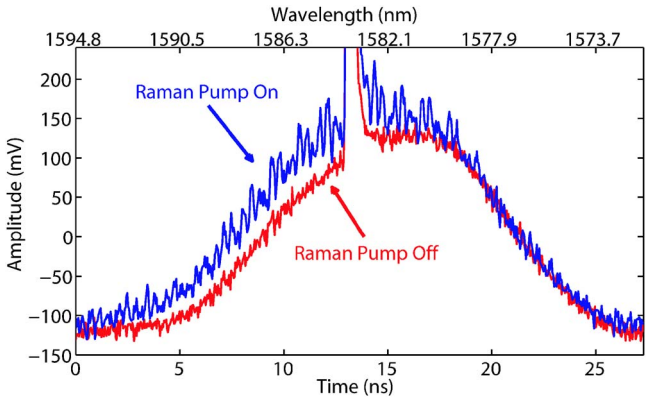

FIG. 3. (Color online) Single-shot interference spectrum measured on a digital oscilloscope, with and without the Raman amplification. The sample is a partial reflector with two layers (both with about −60 dB reflectivity) at imaging depths of 6.6 and 9.1 mm. The spectrum is mapped into the time-domain waveform by the dispersive FT. Raman amplification improves the fringe visibility, which is otherwise invisible. The spikes at 13 ns are due to the reflection of the input beam from the 50/50 fiber coupler without going into the interferometer and are removed from the spectra before inverse FT. The calibrated wavelength axis is shown above the figure.

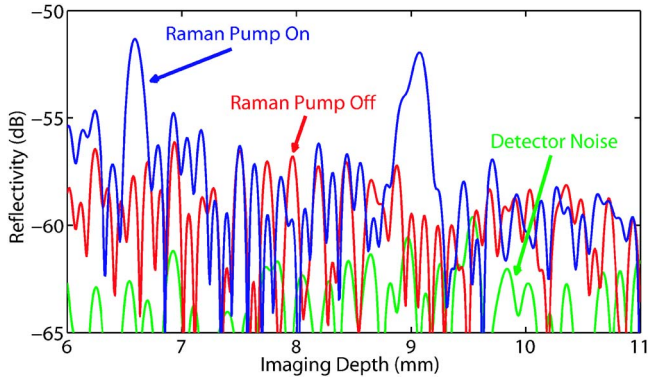

FIG. 4. (Color online) Depth profile of the sample obtained by performing inverse FT on the pulses in Fig. 3. The depth profile only becomes visible with the Raman amplification.

using a supercontinuum source with a much broader bandwidth. To avoid temporal pulse overlap—after dispersion—this will require a proportional reduction in the pulse repetition rate. As an example, a source with a 150 nm bandwidth will give an axial resolution of 22.7 μm (with a theoretical limit of 7.4 μm) while still achieving an axial scan rate of 3.66 MHz.

Figure 3 shows the single-shot spectrum of an interferometer output pulse (with and without the Raman amplification) encoded using a sample with multiple reflecting layers. The sample consists of a weakly reflecting transparent thin film and a weakly reflecting mirror that is located 2.5 mm apart from the film. The incident light is focused onto the film so that the mirror reflection coupled back into the fiber is about −60 dB of the light incident on it. The amplification scheme utilizes two diode lasers to create Raman gain across the signal bandwidth, as described above. The amplification improves the fringe visibility of the interferometer, which is otherwise buried in noise.

Figure 4 shows the depth profile obtained by performing inverse FT on the pulse in Fig. 3. The depth profile, which is otherwise buried in detector noise (hence, invisible), becomes visible due to the amplification. Although signals in both directions (to and from the sample) pass through the amplifier, only the return signal is effectively amplified—the incident signal is not amplified significantly because its peak power is much larger than the pump power supplied to the Raman amplifier.

In conclusion, we have demonstrated improved sensitivity by using distributed Raman postamplification of the reflection from the sample in dispersive FT reflectometry to overcome the fundamental tradeoff between dispersion and loss. The Raman postamplification brings the system closer to the shot noise limit. Raman-amplified reflectometry can be extended to any wavelength band where dispersive elements and Raman pump lasers are available. Balanced detection[4] can also be incorporated into Raman-amplified OFDR and OCT to further increase the detection sensitivity. The sensitivity can also be improved by multishot time-integrated detection and averaging. While the sensitivity enhancement factor is moderate in this proof-of-principle demonstration, the use of more powerful Raman pumps or a fiber with higher Raman gain coefficient can enhance the sensitivity significantly.

This work was partially supported by DARPA. We are grateful to Shalabh Gupta at UCLA for valuable discussions.

[1]N. Tanno, T. Ichikawa, and A. Saeki, Japanese Patent No. 2,010,042 (1990).
[2]D. Huang, E. A. Swanson, C. P. Lin, J. S. Schuman, W. G. Stinson, W. Chang, M. R. Hee, T. Flotte, K. Gregory, C. A. Puliafito, and J. G. Fujimoto, Science **254**, 1178 (1991).
[3]J. G. Fujimoto, Nat. Biotechnol. **21**, 1361 (2003).
[4]D. C. Adler, Y. Chen, R. Huber, J. Schmitt, J. Connolly, and J. G. Fujimoto, Nat. Photonics **1**, 709 (2007).
[5]R. Leitgeb, C. K. Hitzenberger, and A. F. Fercher, Opt. Express **11**, 889 (2003).
[6]M. Wojtkowski, V. Srinivasan, T. Ko, J. Fujimoto, A. Kowalczyk, and J. Duker, Opt. Express **12**, 2404 (2004).
[7]J. D. Jackson, *Classical Electrodynamics* (Wiley, New York, 1999).
[8]J. Chou, D. Solli, and B. Jalali, Appl. Phys. Lett. **92**, 111102 (2008).
[9]D. R. Solli, J. Chou, and B. Jalali, Nat. Photonics **2**, 48 (2008).
[10]R. E. Saperstein, N. Alic, S. Zamek, K. Ikeda, B. Slutsky, and Y. Fainman, Opt. Express **15**, 15464 (2007).
[11]S. Moon and D. Y. Kim, Opt. Express **14**, 11575 (2006).
[12]K. König, P. T. C. So, W. W. Mantulin, and E. Gratton, Opt. Lett. **22**, 135 (1997).
[13]M. N. Islam, IEEE J. Sel. Top. Quantum Electron. **8**, 548 (2002).
[14]P. Jayavel, T. Amano, D. Choi, H. Furukawa, H. Hiro-Oka, K. Asaka, and K. Ohbayashi, Jpn. J. Appl. Phys., Part 2 **45**, L1317 (2006).
[15]B. Rao, J. Zhang, Q. Wang, and Z. Chen, Proc. SPIE **6429**, 642924 (2007).
[16]R. Huber, M. Wojtkowski, K. Taira, J. G. Fujimoto, and K. Hsu, Opt. Express **13**, 3513 (2005).